

# Improved Empirical Parametrization of Fragmentation Cross Sections

K. Sümmerer<sup>1</sup>

<sup>1</sup>*GSI Helmholtzzentrum für Schwerionenforschung, Planckstr.1, D-64291 Darmstadt, Germany*  
(Dated: May 21, 2019)

A new version is proposed for the universal empirical formula, EPAX, which describes fragmentation cross sections in high-energy heavy-ion reactions. The new version, EPAX 3, can be shown to yield cross sections that are in better agreement with experimental data for the most neutron-rich fragments than the previous version. At the same time, the very good agreement of EPAX 2 with data on the neutron-deficient side has been largely maintained. Comparison with measured cross sections show that the bulk of the data is reproduced within a factor of about 2, for cross sections down to the pico-barn range.

PACS numbers: PACS: 25.70.Mn, 25.70.Pq, 25.75.-q

## I. INTRODUCTION

During the last two decades, projectile fragmentation and separation at high energies has become one of the most important methods for the production of exotic nuclei. Production and separation of such species can be performed at energies of around 500 to 1000  $A$  MeV at the SIS/FRS facility [1] at GSI in Darmstadt, Germany. At RIKEN in Wako, Japan, the RIBF facility with the BigRIPS separator [2] allows to perform such experiments at energies of up to 350  $A$  MeV. Considerably lower energies of up to 140  $A$  MeV are attained at the A1900 separator [3] at NSCL in East Lansing, USA, whereas the GANIL/LISE facility at Caen, France, operates below about 80  $A$  MeV [4]. In all cases, the main advantage of high-energy projectile fragmentation as a production method lies in the fact that very clean fragment beams can be produced; the contaminants become less and less important with increasing energy. Moreover, the high energies allow unambiguous event-by-event isotope identification of the fragments produced. Again, the higher energies help in suppressing unwanted charge states of the fragments.

All of the above-mentioned facilities rely on good estimates of fragmentation cross sections in order to predict the production rates of exotic nuclei, together with ion-optical transmission calculations with codes like MO-CADI [5] or LISE++ [6]. One important tool to predict fragmentation cross sections is a universal analytical formula called EPAX [7, 8]. This formula allows to calculate the yields from fragmenting all non-fissile projectiles in the range of projectile masses,  $A_p$ , between about 40 to 209. In particular, the formula tries to take properly into account the influence of the projectile proton or neutron excess onto the neutron-to-proton ratio of the fragments. The cross sections are assumed to be energy-independent, which seems to be supported by most of the measured data, even though no systematic studies of the bombarding-energy dependence have been performed for targets like  $^9\text{Be}$ . The EPAX parametrization aims at reproducing the bulk of the measured cross sections within a factor of two for fragment masses down to about half

the projectile mass. This latter restriction is no severe limitation since the highest transmission in an ion-optical projectile-fragment separator is always attained for small mass and charge differences between projectiles and fragments.

The previous version of the formula, EPAX 2 [8], has proven to give rather realistic estimates of many production cross sections of exotic nuclei. As an example, the very proton-rich fragment  $^{100}\text{Sn}$  was produced with  $11.2 \pm 4.7$  pb [10] in  $^{124}\text{Xe} + ^9\text{Be}$  (later remeasured to yield  $5.8 \pm 2.1$  pb by Straub *et al.* [11]), not far from the EPAX 2 prediction of 7.4 pb. On the other hand, large discrepancies with measured data were found for extremely neutron-rich nuclei like, e.g., fragment yields from 1  $A$  GeV  $^{136}\text{Xe} + ^9\text{Be}$ , which were overestimated by EPAX by up to two orders of magnitude [12]. It is therefore desirable to try and modify the EPAX 2 parameters in such a way that also the yields of very neutron-rich fragments of medium- and heavy-mass projectiles can be predicted with better accuracy.

In the following, the basic characteristics of the EPAX formula will be reviewed. This is followed by an explanation how the parameters of EPAX can be obtained by fits to recent data sets. These fits allow to get a feeling how the EPAX parameters vary with fragment mass and with proton or neutron excess of the projectile. The final choice of the parameters for EPAX 3 is then presented, together with comparisons between measured data of selected systems and the predictions of the new parametrization.

## II. THE EPAX FORMULA

As explained in detail in Ref. [8], the cross section  $\sigma$  of a fragment with mass  $A$  and charge  $Z$  produced by projectile fragmentation from a projectile ( $A_p, Z_p$ ) impinging on a target ( $A_t, Z_t$ ) is written as

$$\sigma(A, Z) = Y_A \sigma_Z(Z_{prob} - Z) = Y_A n \exp(-R |Z_{prob} - Z|^U). \quad (1)$$

The first term,  $Y_A$ , represents the mass yield, i.e. the sum of all isobaric cross sections with fragment mass  $A$ .

The second term,  $\sigma_Z$ , describes the "charge dispersion", the distribution of elemental cross sections with a given mass,  $A$ , around its maximum,  $Z_{prob}$ . The shape of the charge dispersion is controlled by the width parameter,  $R$ , and the exponent,  $U$ . The factor  $n = \sqrt{R/\pi}$  simply serves to normalize the integral of the charge dispersion approximately to unity. Note that the isobar distributions are not symmetric on the neutron- and proton-rich side, therefore  $U$  has two different values,  $U_p$  and  $U_n$ , on the proton- and neutron-rich side of the valley of  $\beta$ -stability, respectively. In Ref. [8], the exponent  $U$  for the neutron-rich side of the isobar distribution was chosen as  $U_n = 1.65$ . In the present version, the exponent on the proton-rich side is also taken as a constant,  $U_p = 2.1$ , close to the value of 2.0 for a Gaussian. Thus, in a fitting procedure of the EPAX parameters to measured data, three parameters have to be obtained for each fragment mass,  $A$ : An amplitude constant, proportional to the mass yield,  $Y_A$ , the centroid of the charge dispersion,  $Z_{prob}$ , and the width parameter,  $R$ . As was shown in Ref. [8], a fourth parameter has to be determined for those data sets where small cross sections of very proton-rich fragments have been measured: the transition point,  $Z_{exp}$ , where the quasi-Gaussian shape of the charge dispersion on the proton-rich side turns into an exponential decay.

### A. EPAX fits to measured data sets

During the decade between the release of EPAX 2 and today, many data-sets of experimental fragmentation cross-sections have been published, some of them very comprehensive in their coverage of fragment charge and mass numbers. In addition to the experiments cited in the EPAX 2 paper [8] and the ones mentioned above [9, 10], very comprehensive data on the fragmentation of  $^{40,48}\text{Ca}$  and  $^{58,64}\text{Ni}$  on  $^9\text{Be}$  and  $^{181}\text{Ta}$  targets at 140  $A$  MeV by Mocko *et al.* [13] turned out very useful. Tarasov *et al.* [14] have published a very careful study of  $^{76}\text{Ge}$  fragmentation at 132  $A$  MeV, where great care was taken to reliably model the (relatively small) transmission of the MSU A1900 separator at this bombarding energy. Data for heavier projectiles, all on  $^9\text{Be}$  targets, were measured at the FRS separator at GSI [1]: For  $^{92}\text{Mo}$  (at 500  $A$  MeV) by Fernandez *et al.* [15], for  $^{112}\text{Sn}$  by Stolz *et al.* [16], and for  $^{208}\text{Pb}$  by Benlliure *et al.* [17], the latter all measured at 1  $A$  GeV. In addition, a very comprehensive data set for  $^{124,136}\text{Xe}$  on a  $^{208}\text{Pb}$  target, again at 1  $A$  GeV, has been published by Henzlova *et al.* [19]. A remarkable milestone was reached by Perez and co-workers [20] who succeeded to measure a rather large set of fragmentation cross sections for a secondary beam of the extremely neutron-rich nucleus  $^{132}\text{Sn}$ , obtained from  $^{238}\text{U}$  projectile fragmentation at 1  $A$  GeV.

In a few cases, cross sections for the same fragment have been measured at both, medium and high bombarding energies. A very comprehensive data set is avail-

able for the projectile  $^{58}\text{Ni}$ , with data measured at 140  $A$  MeV [13] and at 650  $A$  MeV [21]. The experimental cross sections agree well within their respective error bars, therefore the 140  $A$  MeV data sets for  $^{40,48}\text{Ca}$  and  $^{58,64}\text{Ni}$  on  $^9\text{Be}$  of Ref. [13] were included in the fits of Eq. (1) to isobaric cross section distributions.

It turns out that Eq. (1) can describe the distributions with very good accuracy over many orders of magnitude. The significance of a good fit is high, however, only for distributions where many data points on both, the proton and neutron rich side are available. If only few data points are available for a given  $A$  and, in particular, if only one side of the charge dispersion has been measured, it is difficult to obtain a unique set of fit parameters since the parameters are strongly correlated. A good example is visualized in Fig. 1, where Eq. (1) has been fitted to data for 9 different isobars of the  $A = 50$  mass chain, where 3 cross sections have been measured at both energies, 140  $A$  MeV [13] and at 650  $A$  MeV [21]. The smallest cross sections measured amount to sub-nanobarns. Note that on the proton-rich side the quasi-Gaussian with

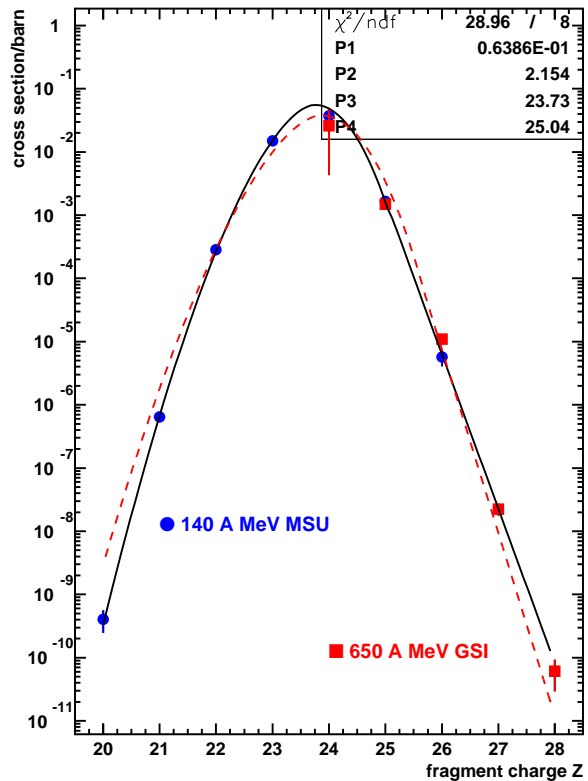


FIG. 1. (color online) Experimental cross sections for  $A = 50$  isobars from  $^{58}\text{Ni}$  fragmentation at 140  $A$  MeV (Ref. [13], circles) and at 650  $A$  MeV (Ref. [21], squares) in a  $^9\text{Be}$  target. The full curve represents a least-squares fit of Eq. (1) to the data. The dashed curve shows the agreement of the EPAX 3 formula with the data.

an exponent of  $U_p = 2.1$  turns to an exponential slope at  $Z_{exp} = 25.04$ .

Fits of this type can be made for all of the systems

of Refs. [13, 17, 19, 21] for those isobaric chains where at least 4 data points are available. For  $^{208}\text{Pb}$ , the data measured with a  $^{nat}\text{Cu}$  target by De Jong *et al.* [22] were combined with those measured with a  $^9\text{Be}$  target by Benliure *et al.* [17] by scaling the former ones with a scaling factor of 0.77 to account for the larger size of the Cu target (see Eq. (3) below). For most of the systems, three parameters were used in EPAX fits to isobaric cross section distributions. Only for  $^{58}\text{Ni}$ , the smallest cross sections on the proton-rich side required the inclusion of a fourth parameter,  $Z_{exp}$ . Examples of the fragment-mass dependence of the parameters  $Y_A$ ,  $Z_{prob}$ , and  $R$  are given below in Figs. 3-5.

## B. The EPAX 3 formula and its parameters

### 1. Mass yields

As noted already in Ref. [7], the mass-yield curve,  $Y_A(A)$ , can be simply approximated by an exponential depending on the difference between projectile and fragment masses,  $(A_p - A)$ . The slope of this exponential,  $P$ , is a function of the projectile mass only. The functional form of the mass yield curve in EPAX 3 has been kept identical to the previous version:

$$Y_A = S \cdot P \cdot \exp(-P \cdot (A_p - A)), \quad (2)$$

$$S = s_1 \cdot (A_p^{1/3} + A_t^{1/3} - s_2) \text{ [barn]}, \quad (3)$$

$$P = \exp(p_1 + p_2 \cdot A_p). \quad (4)$$

Eq. 3 shows that the dependence of  $S$  on the sum of  $A_t^{1/3}$  and  $A_p^{1/3}$  and thus on the circumference of the colliding nuclei has been kept. As the only change the overlap factor,  $s_2$ , has been slightly reduced from 2.38 to 1.8 fm. Results from a recent paper on charge-changing cross sections induced by 650 A MeV  $^{40}\text{Ar}$  and 1 A GeV  $^{48}\text{Ti}$  ions by Zeitlin *et al.* [18] confirm that Eq. 3 is a good description of the geometrical scaling factor. Fig. 2 shows the ratios of charge-changing cross sections for Al, Cu, Sn, and Pb targets, relative to those of a carbon target, and averaged over all charge changes measured in Ref. [18]. The x-axis corresponds to the scaling variable in Eq. 3,  $(A_p^{1/3} + A_t^{1/3} - s_2)$ ; the straight line represents Eq. 3. In Ref. [8] it was shown that the mass yield  $Y_A$  has to be increased near the projectile (see Eq. (13) of Ref. [8]). The same formula was kept for the new Version 3:

$$Y'_A = Y_A \cdot [y_2 \cdot A_p \cdot (x - y_1)^2] \quad (5)$$

for  $x \geq y_1$ ;  $x$  is the ratio of fragment mass to projectile mass,  $x = A/A_p$ . The numerical values of all constants can be found in Table I.

Typical examples of mass yields are shown in Fig. 3. One can clearly see that the slopes,  $P$ , are much steeper for lighter projectiles like  $^{58,64}\text{Ni}$  than for heavier ones like  $^{124,136}\text{Xe}$ . An inspection of Eq. (5) shows that the upward bend of  $Y_A(A)$  towards the projectile mass scales

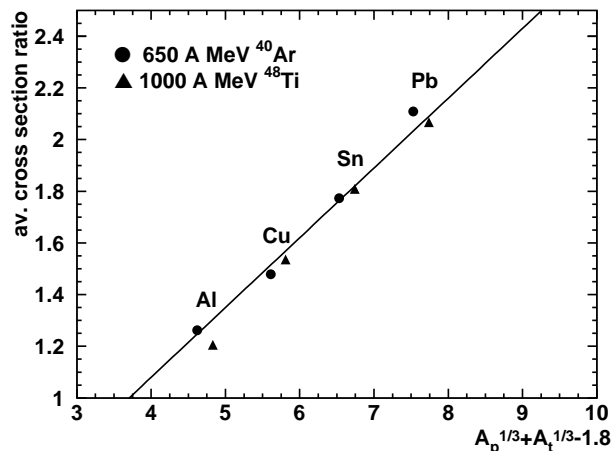


FIG. 2. Charge-changing cross sections of relativistic  $^{40}\text{Ar}$  and  $^{48}\text{Ti}$  beams interacting with the targets indicated in the figure, relative to those with C targets. The ratios were averaged over all charge changes measured in Ref. [18]. The straight line represents the EPAX description, Eq. 3.

with  $A_p$  and thus has only a minor effect on the  $^{58,64}\text{Ni}$  mass yield distributions. The slope differences between each of the two Ni and Xe isotope pairs are entirely due to the  $A_p$ -dependence of  $P$ .

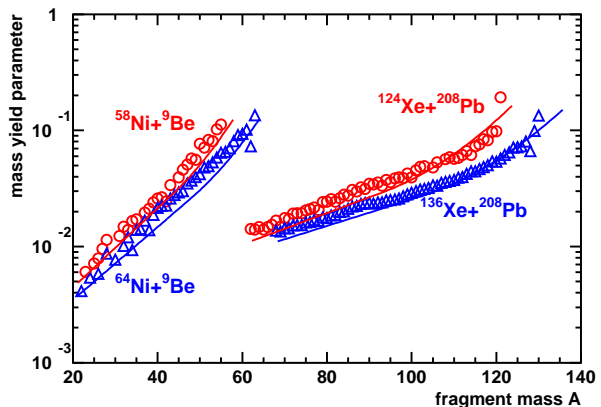


FIG. 3. (color online) Mass yields,  $Y_A(A)$ , for  $^{58,64}\text{Ni}+^9\text{Be}$  and  $^{124,136}\text{Xe}+^{208}\text{Pb}$ . The open symbols are derived from EPAX fits to the experimental data of Refs. [13, 19]. The full lines have been calculated from Eqs. (2-5).

### 2. Centroid $Z_{prob}$

As mentioned above, the charge dispersion is mainly characterized by its centroid,  $Z_{prob}$ , and its width parameter,  $R$ . As in EPAX Versions 1 and 2, the loci of maximum cross section,  $Z_{prob}(A)$ , have been parameter-

ized relative to the valley of  $\beta$ -stability,

$$Z_{prob} = Z_{\beta} + \Delta + \Delta_m. \quad (6)$$

$Z_{\beta}$  is approximated by the smooth function

$$Z_{\beta} = A / (1.98 + 0.0155 \cdot A^{2/3}). \quad (7)$$

$\Delta$  is found to be a linear function of the fragment mass,  $A$ , for heavy fragments ( $A \geq d_4$ ), and is extrapolated quadratically to zero:

$$\Delta = \begin{cases} d_1 + d_2 \cdot A & \text{if } A \geq d_4 \\ d_3 \cdot A^2 & \text{if } A < d_4 \end{cases} \quad (8)$$

The sum  $Z_{\beta} + \Delta$  defines the “residue corridor”, the locus in the  $A - Z$  plane where the fragments from all projectiles located near  $\beta$ -stability end up after long evaporation chains. This corridor is close to the line Charity [23] has found from studying the residue distributions after evaporation from highly excited compound nuclei (see dashed line in Fig. 4 and Eqs.(6,7) in Ref. [23]). This points to the fact that the fragment distributions far away from the projectiles are largely controlled by evaporation from equilibrated pre-fragments.

It is obvious that close to the projectile  $Z_{prob}$  has to move away from the corridor and approach  $Z_p$ , i.e., for projectiles located on the line of  $\beta$ -stability  $\Delta$  has to

Parameter	Constant	Value
Scaling factor $S$	$s_1$	0.27
	$s_2$	1.80
Mass yield slope $P$	$p_1$	-1.731
	$p_2$	-0.01399
Mass yield correction factor	$y_1$	0.75
	$y_2$	0.10
$Z_{prob}$ shift $\Delta$	$d_1$	-1.087
	$d_2$	$3.047 \cdot 10^{-2}$
	$d_3$	$2.135 \cdot 10^{-4}$
	$d_4$	71.35
	$d_5$	-25.0
	$d_6$	0.80
n-rich memory effect $\Delta_m^n$	$n_1$	0.40
	$n_2$	0.60
p-rich memory effect $\Delta_m^p$	$q_1$	-10.25
	$q_2$	10.25
n-rich slope $U_n$	$U_n$	1.65
p-rich slope $U_p$	$U_p$	2.10
Width parameter $R$	$r_0$	2.78
	$r_1$	-0.015
	$r_2$	$3.20 \cdot 10^{-5}$
	$r_3$	0.0412
	$r_4$	0.124
	$r_5$	30.0
	$r_6$	0.85
Transition point to exponential slope	$l_1$	1.20
	$l_2$	0.647
Downscale factor	$b_1$	$2.3 \cdot 10^{-3}$
	$b_2$	2.4

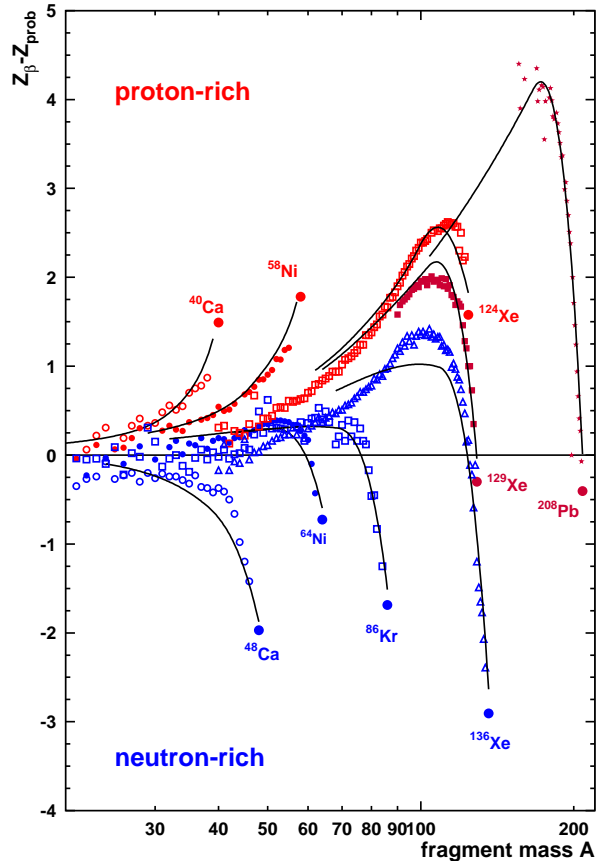


FIG. 4. (color online) Loci of the peak cross sections,  $Z_{prob}(A)$ , as a function of fragment mass, for various projectiles as indicated in the Figure. For clarity, the value of  $Z_{\beta}(A)$  has been subtracted at each mass number  $A$ . The data points have been obtained by fitting Eq. (1) to isobaric distributions for the systems indicated. Positive (negative)  $y$ -values correspond to proton-rich (neutron-rich) nuclei relative to  $Z_{\beta}$ . The large dots indicate where the respective projectile is located in this graph. The lines represent the EPAX predictions according to Eqs. (6-11).

approach zero. That has been achieved by the following modification

$$\Delta' = \Delta \cdot [1 + d_5 \cdot (x - d_6)^2] \quad (9)$$

if  $x > d_6$ .

For projectiles on the proton- or neutron-rich side of the valley of  $\beta$ -stability, an additional correction of  $Z_{prob}$  is necessary, which accounts for the “memory effect”, the gradually vanishing proton or neutron excess of the fragment reflecting the proton or neutron excess of the projectile,  $(Z_p - Z_{\beta p})$ , where  $Z_{\beta p}$  is the value of Eq. 7 for the projectile,  $A = A_p$ . This additional correction, termed  $\Delta_m$  in Eq. (6), should reflect the full excess at the projectile mass and should gradually approach zero with increasing mass loss from the projectile. The functional forms have been kept as in the previous version,

$$\Delta_m^n = (n_1 \cdot x^2 + n_2 \cdot x^4) \cdot (Z_p - Z_{\beta p}) \quad (10)$$

for neutron-rich projectiles, and

$$\Delta_m^p = \exp(q_1 + q_2 \cdot x) \cdot (Z_p - Z_{\beta p}) \quad (11)$$

for proton-rich projectiles. In both cases, the choice of the parameters guarantees the limiting properties mentioned above.

Fig. 4 visualizes how the combined effects of  $\Delta$ ,  $\Delta'$ , and  $\Delta_m$  compare to data of  $(Z_\beta(A) - Z_{prob}(A))$  derived from EPAX fits to the experimental data sets of Refs. [13, 19, 24, 25]. The zero line corresponds to the line of  $\beta$ -stability according to Eq. (7). The full lines have been calculated using Eqs. (6-11). The agreement with the fitted data points is rather good close to the projectile masses; further away, one notes bad agreement in particular for  $^{136}\text{Xe}$ .

### 3. Width parameter $R$

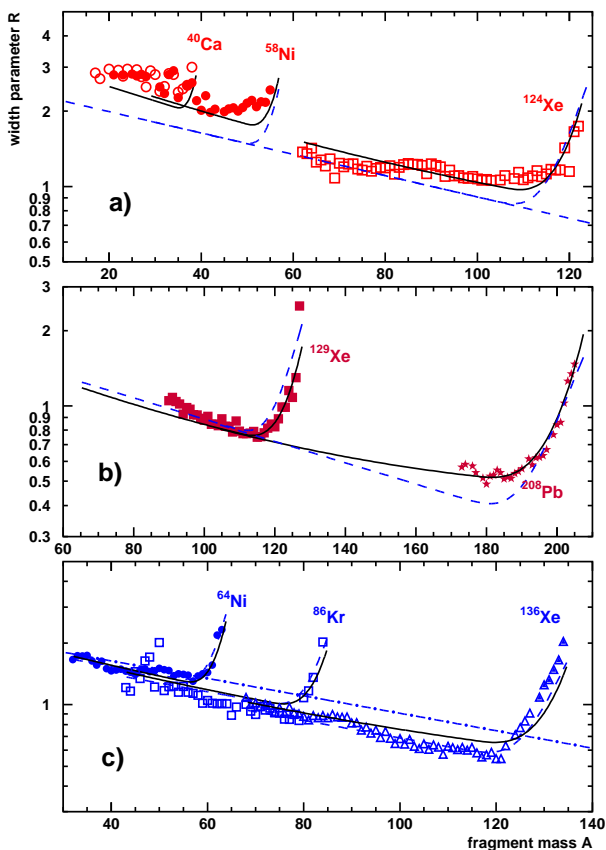


FIG. 5. (color online) (a) Fragment-mass dependence of the width parameter,  $R$ , for proton-rich projectiles. The dashed curves denote the old EPAX 2 parametrization, while the new Version 3 is indicated by the full curves. (b) The same for projectiles near the line of  $\beta$ -stability. Note the reduced widths (larger  $R$  values) for  $^{208}\text{Pb}$ -fragments according to EPAX 3. (c) The same for proton-rich projectiles. Since here the dashed curves are almost invisible, the dash-dotted line indicates the EPAX 2 curve for stable and proton-rich projectiles.

Similar to the parameter  $Z_{prob}$  just discussed, the width parameter,  $R$ , is to first order a function of fragment mass only, irrespective of the projectile. In Ref. [8] it was found that the experimental  $R$ -values can be approximated by a simple exponential (see Eq. (8) of Ref. [8]). As visualized in the following section, this yields too wide charge dispersions for very heavy nuclei, such that now a parabolic dependence in log scale has been chosen:

$$R = R_0 \cdot \exp(r_1 \cdot A + r_2 \cdot A^2) \quad (12)$$

It was already noted in Ref. [8] that the charge dispersions from neutron-rich projectiles are a bit wider than those from proton-rich or  $\beta$ -stable ones. In the present version of EPAX, this has been coded in the following form: the parameter  $R_0$  in Eq. (12) depends differently on the proton and the neutron excess of the projectile:

$$R_0^n = r_0 \cdot \exp[r_3 \cdot (Z_p - Z_{\beta p})] \quad (13)$$

$$R_0^p = r_0 \cdot \exp[r_4 \cdot (Z_p - Z_{\beta p})] \quad (14)$$

It is again obvious that close to the projectile the widths of the charge dispersions should shrink since the smaller number of nucleons removed from the projectile also reduces the variance of the mass loss. Therefore, the following modification has been introduced near the projectile, i.e. for  $x > r_6$ :

$$R' = R \cdot \exp[r_5 \cdot \sqrt{A_p} \cdot (x - r_6)^3]. \quad (15)$$

The  $\sqrt{A_p}$ -dependence of the pre-factor in the exponent guarantees a small effect for light and a stronger one for heavy projectiles.

Fig. 5 compares the resulting width parameters  $R$  from Eqs. (12-15) to fitted data. The upper part, (a), shows this comparison for proton-rich projectiles ( $^{40}\text{Ca}$ ,  $^{58}\text{Ni}$ , and  $^{124}\text{Xe}$ ). The EPAX 3 parametrization (full lines) leads to more narrow charge dispersions than the EPAX 2 one (dashed lines). Fig. 5b has been plotted for the projectiles  $^{129}\text{Xe}$  and  $^{208}\text{Pb}$ , both located close to the line of  $\beta$ -stability. The more narrow widths compared to the previous parametrization [8] for  $^{208}\text{Pb}$  are clearly visible. The lower panel, (c), displays  $R(A)$  for three neutron-rich projectiles,  $^{64}\text{Ni}$ ,  $^{86}\text{Kr}$ , and  $^{136}\text{Xe}$ . The parametrization according to EPAX 2 coincides with the data points and is hardly visible; there is not much difference to the Version 3 parametrization (full lines). The dash-dotted line indicates the EPAX 2 exponential for stable or proton-rich projectiles; it is obvious that neutron-rich projectiles lead to considerably wider distributions.

### 4. Modifications for very proton-rich fragments

A major modification of EPAX 2 compared to EPAX 1 consisted in the introduction of an exponential rather than a quasi-Gaussian shape of the charge distribution beyond a certain transition point on the proton-rich

side [8]. This was coded by calculating the derivative of the logarithm of the cross section (Eq. (1)):

$$\frac{dF}{dZ} = \frac{d(\log(\sigma))}{dZ} \approx \frac{-2 \cdot R}{\ln(10)} \cdot (Z - Z_{prob}) \quad (16)$$

The transition point to the exponential slope,  $Z_{exp}$ , has been calculated for the proton-rich side as a function of the fragment mass  $A$  according to

$$Z_{exp}(A) = Z_{prob}(A) + \left. \frac{dF}{dZ} \right|_A \cdot \frac{\ln(10)}{2 \cdot R(A)} \quad (17)$$

From  $Z_{exp}$  on, the slope is exponential with the same gradient as Eq. (1) at this point. The empirical parametrization for the transition slope proposed in Ref. [8],

$$\frac{dF}{dZ} = l_1 + l_2 \cdot (A/2)^{0.3} \quad (18)$$

not only yields perfect agreement with very proton-rich fragments from  $^{58}\text{Ni}$ , but provides the same quality also for fragments from  $^{124}\text{Xe}$ , e.g. for  $^{100}\text{Sn}$ , for which EPAX 2 calculates a cross section of 7.4 pb, whereas Straub *et al.* measure  $5.8 \pm 2.1$  pb [11]. This parametrization has therefore been kept in EPAX 3, the  $^{100}\text{Sn}$  cross section from this new version now amounts to 6.9 pb.

#### 5. Modifications for very neutron-rich fragments

It has been noted by several authors (e.g. by Benlliure *et al.* [12, 17]) that EPAX 2 overestimates cross sections of very neutron rich fragments from, e.g.,  $^{136}\text{Xe}$  or  $^{208}\text{Pb}$  by up to two orders of magnitude. After many failed attempts to modify the EPAX parameters in such a way that the discrepancies were removed, it became clear that only a “brute-force solution” could solve this problem. This means that all cross sections from neutron-rich projectiles calculated by EPAX 3 with Eqs. (1-18) above should be downscaled by a factor that depends on both, the neutron excess of the projectile and the fragment. This “brute-force factor” can be written as

$$f_{bf} = 10^{[B \cdot (Z_\beta(A) - Z + b_2)^3]} \quad (19)$$

$$B = -b_1 \cdot |Z_p - Z_{\beta p}| \quad (20)$$

where  $Z_\beta$  and  $Z_{\beta p}$  are the values of Eq. (7) for fragment mass  $A$  and projectile mass  $A_p$ , respectively. It applies to fragments where  $(Z_\beta - Z) > (Z_p - Z_{\beta p} + b_2)$ . The effect of this factor is quite dramatic for the most neutron-rich fragments of heavy projectiles as will be shown below.

### III. COMPARISONS WITH EXPERIMENTAL CROSS SECTIONS

#### A. Projectiles close to $\beta$ -stability

An important testing ground for the quality of EPAX 3 predictions are the fragmentation cross sections of

$^{208}\text{Pb}$ , one of the few heavy projectiles to explore the yet poorly studied region in the chart of nuclides “south” and “south-east” of this nucleus. Data were measured at 1 A GeV bombarding energy on  $^{nat}\text{Cu}$  [22] and  $^9\text{Be}$  [17] targets. For the following comparison (Fig. 6) the cross sections of Ref. [22] were scaled by a factor of 0.78 according to Eq. (3). Both data sets fit excellently to each other and are well reproduced over a large range of fragment masses by EPAX 3. In particular, the predictions for neutron-rich fragments farther away from the projectile are now much closer to the experimental data than those of EPAX 2. Small discrepancies remain for the most neutron-rich Tl and Hg isotopes.

#### B. Fragmentation of neutron-rich projectiles

It was mentioned in the Introduction that one of the most severe deficiencies of EPAX 2 was its overprediction of cross sections of very neutron-rich fragments, e.g. those from  $^{136}\text{Xe} + ^9\text{Be}$  [12]. It is therefore interesting to see the effect of the new parameters and in particular that of the “brute-force” downscale factor (Eq. (19,20)). Some isotope distributions from this system are shown in Fig. 7. The flat isotope distribution for  $Z = 53$  is not so well reproduced, but for the bulk of the cross sections of very neutron-rich fragments EPAX 3 fits better than the previous version. For the few data points measured for  $Z = 45$ , the new description seems even to underpredict slightly the data.

Similar conclusions can be drawn if one plots the cross sections for the proton-loss channels with  $N = 82$  from  $^{136}\text{Xe} + ^9\text{Be}$  (Fig. 8). Benlliure *et al.* have noted in Ref. [12] that EPAX 2 yields too flat a slope for the cross sections of the  $N = 82$  isotones. Fig. 8 now demonstrates that the new parametrization gives a slope in very good agreement with measured data, despite a discrepancy, however, at  $Z = 53$ .

Fig. 8 compares EPAX 3 also to the predictions of a physical model, the “cold fragmentation” model COFRA [26]. This model, a simplified analytical version of the abrasion-ablation model which is valid in regions where only neutron evaporation plays a role, has been shown to reproduce the cross sections of many neutron-rich fragments very well (see, e.g., Refs. [12, 17, 20]). The same is true for the  $Z = 50 - 53$  data points in Fig. 8. The model tends to slightly underpredict, however, the lowest- $Z$  data points, where EPAX 3 seems to follow the data a bit better.

#### C. Fragmentation of proton-rich projectiles

Contrary to the neutron-rich fragments discussed in the previous subsection, cross sections for even extremely proton-rich fragments like  $^{48}\text{Ni}$  or  $^{100}\text{Sn}$  were already predicted with surprising accuracy by EPAX 2. Care was undertaken in the present study not to deteriorate



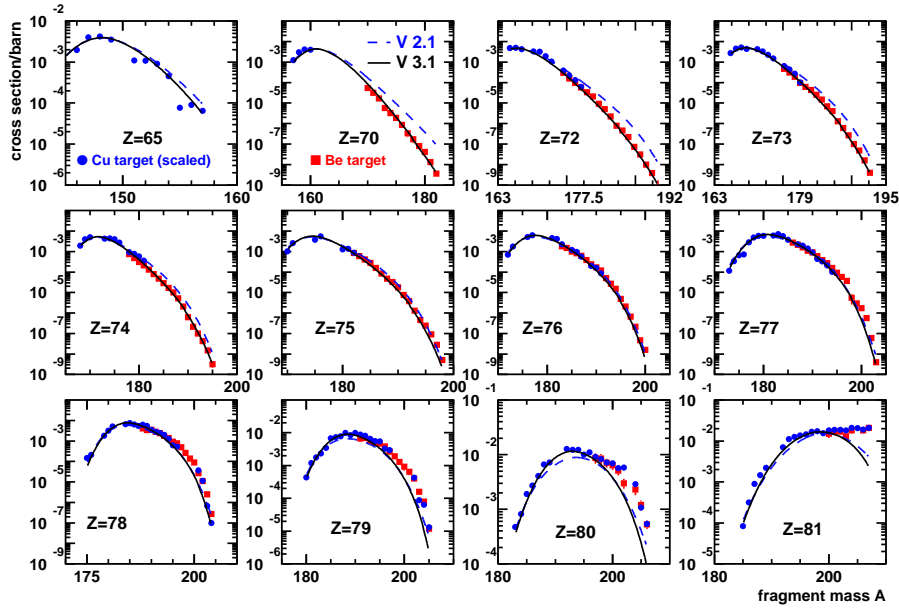


FIG. 6. (color online) Isotope distributions from 1 A GeV  $^{208}\text{Pb}$  fragmentation in a  $^{nat}\text{Cu}$  (circles, Ref. [22]) and a  $^9\text{Be}$  (squares, Ref. [17]) target. The Cu-target data were scaled by a factor of 0.77 according to Eq. (3). The full line represents the new EPAX 3 parametrization, whereas the dashed line shows the old EPAX 2 version.

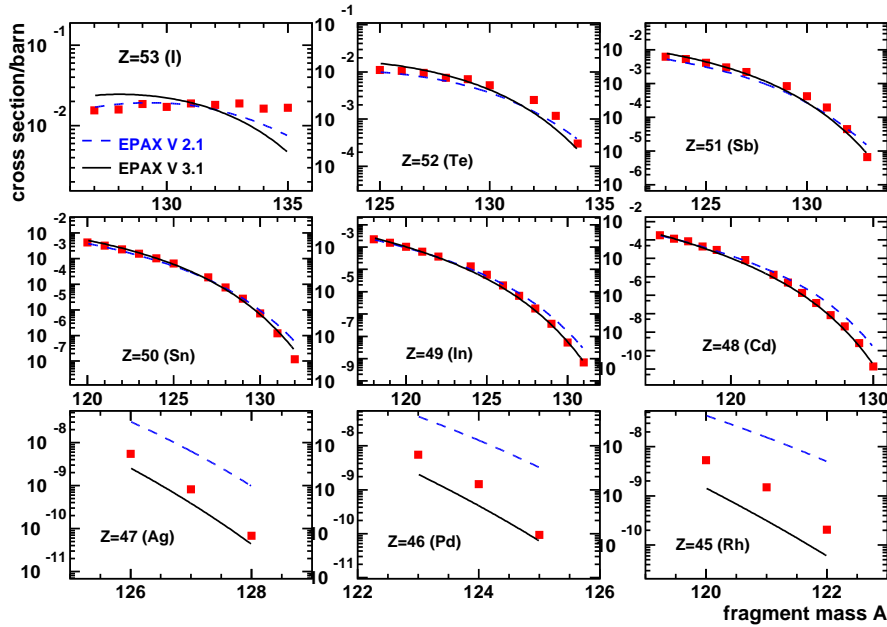


FIG. 7. (color online) Same as Fig. 6 but for the system  $^{136}\text{Xe}+^9\text{Be}$  [12]. EPAX 3 behaves worse than EPAX 2 very close to the projectile but fits better to the measured data points for most of the very neutron-rich fragments.

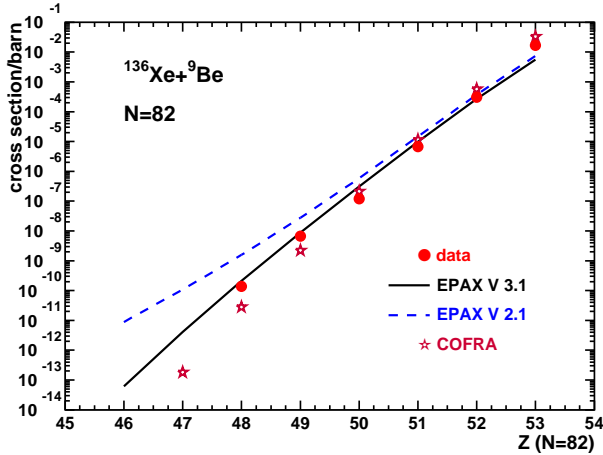


FIG. 8. (color online) Cross sections of proton-loss channels for 1 A GeV  $^{136}\text{Xe}$  on  $^9\text{Be}$  (dots, Ref. [12]) in comparison with EPAX 3 (full line), EPAX 2 (dashed curve) and with the physical “cold fragmentation” model COFRA [26] (stars).

the excellent predictive power of EPAX on the proton-rich side. Fig. 9 shows that this has been achieved to a large extent. The figure shows measured cross sections for  $^{112}\text{Sn}+^9\text{Be}$  [16], complemented by data for less exotic fragments from the system  $^{112}\text{Sn}+^{112}\text{Sn}$  [27], both data sets obtained at 1 A GeV. The Sn-target data were scaled by a factor of 0.65 (Eq. 3) to match the Be-target data. Fig. 9 confirms that both data sets fit together smoothly and that EPAX 3 describes the entire distributions rather well, very similar to EPAX 2. As a benchmark test, one can check the cross section of  $^{100}\text{Sn}$  from  $^{112}\text{Sn}+^9\text{Be}$  fragmentation: The agreement with the measured value of  $1.8^{+2.3}_{-1.3}$  pb [16] has deteriorated a bit, but not much (Version 3 predicts 7.9 pb, compared to 6.6 pb for Version 2). Another benchmark is provided by the fragment  $^{48}\text{Ni}$  produced from  $^{58}\text{Ni}+^{58}\text{Ni}$  at 160 A MeV with a cross section of  $100 \pm 30$  fb [29]. This is to be compared with an EPAX 3 prediction of 20 fb, EPAX 2 predicted 57 fb.

#### D. Range of validity of the EPAX formula

As mentioned in the Introduction, the EPAX parametrization contains no bombarding-energy dependent terms, following the concept of “limiting fragmentation”, which assumes that the cross sections for the formation of fragments rather close to the projectile are independent of bombarding energy if the latter is sufficiently above the Fermi energy in nuclei ( $\approx 40$  A MeV). This concept is difficult to prove since only few systems have been investigated where identical fragments were produced at several different bombarding energies. One system is  $^{58}\text{Ni}+^9\text{Be}$  which was studied at 140 and 650 A MeV [13, 21]. An example how well results from

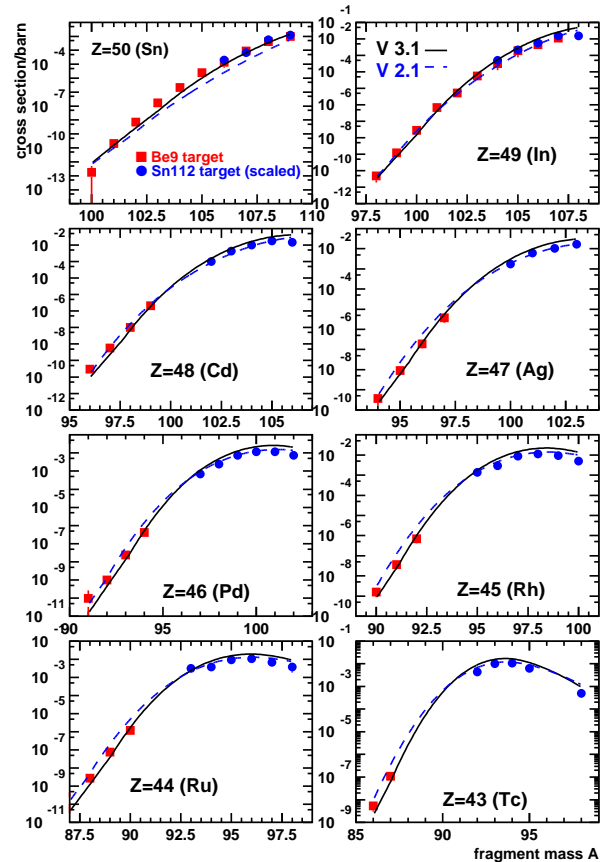


FIG. 9. (color online) EPAX 3 (full lines) and EPAX 2 (dashed lines) predictions for production cross sections from  $^{112}\text{Sn}+^9\text{Be}$ , in comparison with data on a  $^9\text{Be}$  (Ref. [16], squares) and a  $^{112}\text{Sn}$  (Ref. [27], circles) target measured at 1 A GeV. The latter data points have been scaled by a factor of 0.65.

these two studies fit to each other was shown above in Fig. 1; other mass chains exhibit similar agreement. Another study also points to the fact that around 140 A MeV energy independence is largely achieved: the reaction  $^{76}\text{Ge}+^9\text{Be}$  at 132 A MeV studied by Tarasov *et al.* [14]. Most of their cross sections of very neutron-rich fragments in the range  $23 \leq Z \leq 17$  are quantitatively reproduced by EPAX 3.

On the other hand, a comparison of two  $^{86}\text{Kr}$ -induced data sets, one measured at 500 A MeV [24] and the other at 64 A MeV [28], do not yield identical results. EPAX fits to the latter yield systematically narrower width parameters,  $R$ . Moreover, the simple geometrical scaling law for two different targets, which seems to work at high energies (see Figs. 6,9), breaks down as visualized in Fig. 11 of Ref. [28]. In agreement with Mocko *et al.* we conclude that an energy of 64 A MeV is below the range of validity of the EPAX formula.



#### IV. SUMMARY

Some modifications of the EPAX 2 parameters allow to improve the predictive power of the EPAX formula in regions where too large cross sections were calculated, in particular for very neutron-rich fragments from medium-mass and heavy projectiles. In addition to a modified parameter set, a “downscale factor” had to be introduced for neutron-rich projectiles that depends on the neutron-excess of the projectile and scales with the neutron-excess of the fragment. The resulting EPAX 3 formula reproduces with rather good accuracy the bulk of the measured fragmentation cross sections as long as the incident projectile energy is larger than 130 - 140 A MeV. Systematic discrepancies were found for  $^{86}\text{Kr}$  projectiles at 64 A MeV. The improvement of EPAX 3 compared to the previous version is confirmed by the much better agreement with the physical “cold-fragmentation” model

COFRA, which was found to reproduce well measured cross sections for the most neutron-rich fragments from  $^{136}\text{Xe}$  and  $^{208}\text{Pb}$ .

The program code of the EPAX formula can be downloaded from the GSI Document Server [30].

#### ACKNOWLEDGMENTS

Sincere thanks are due to many colleagues who have provided numerical data of their results, sometimes prior to publication. Among them are in particular H. Alvarez Pol, J. Benlliure, D. Henzlova, A. Kelic, J. Kurcewicz, T. Kurtukian Nieto, D. Perez Loureiro, M. Mocko, A. Stolz, O. Tarasov, and B. Tsang. The author acknowledges gratefully the kind hospitality of the Grupo Experimental de Nucleos y Particulas at the Universidad de Santiago de Compostela where part of this work was completed.

- 
- [1] H. Geissel *et al.*, Nucl. Instr. Meth. Phys. Res. **B 70**, 286 (1992).
  - [2] T. Kubo *et al.*, Nucl. Instr. Meth. Phys. Res. **B 204**, 97 (2003).
  - [3] D.J. Morrissey *et al.*, Nucl. Instr. Meth. Phys. Res. **B 204**, 90 (2003).
  - [4] A.C. Mueller and R. Anne, Nucl. Instr. Meth. Phys. Res. **B 56**, 559 (1991).
  - [5] N. Iwasa, H. Geissel, G. Münzenberg, C. Scheidenberger, T. Schwab, and H. Wollnik, Nucl. Instr. Meth. Phys. Res. **B 126**, 284 (1997).
  - [6] O. Tarasov *et al.*, Nucl. Instr. Meth. Phys. Res. **B xxx**, yyy (zzz).
  - [7] K. Sümmerer, W. Brüche, D.J. Morrissey, M. Schädel, B. Szweyryn, and Yang Weifan, Phys. Rev. C **42**, 2546 (1990).
  - [8] K. Sümmerer and B. Blank, Phys. Rev. C **61**, 034607 (2000).
  - [9] B. Blank *et al.*, Phys. Rev. C **84**, 1116 (2000).
  - [10] R. Schneider, Ph.D. thesis (1996).
  - [11] K. Straub, Ph.D. thesis (2010).
  - [12] J. Benlliure *et al.*, Phys. Rev. C **78**, 054605 (2008).
  - [13] M. Mocko *et al.*, Phys. Rev. C **74**, 054612 (2006).
  - [14] O. Tarasov *et al.*, Nucl. Instr. Meth. in Phys. Res. A **620**, 578 (2010).
  - [15] B. Fernandez *et al.*, Eur. Phys. J. A **25**, 193 (2005); *ibid.* 473 (2005).
  - [16] A. Stolz *et al.*, Phys. Rev. C **65**, 064603 (2002).
  - [17] J. Benlliure *et al.*, Eur. Phys. J. Special Topics **150**, 309 (2007).
  - [18] C. Zeitlin *et al.*, Phys. Rev. C **77**, 034605 (2008).
  - [19] D. Henzlova *et al.*, Phys. Rev. C **78**, 044616 (2008).
  - [20] D. Perez Loureiro *et al.*, Phys. Lett. **B 703** (2011) 552.
  - [21] B. Blank *et al.*, Phys. Rev. C **50**, 2398 (1994).
  - [22] M. DeJong *et al.*, Nucl. Phys. **A 628**, 479 (1998).
  - [23] R.J. Charity, Phys. Rev. C **58**, 1073 (1998).
  - [24] M. Weber *et al.*, Nucl. Phys. **A578**, 659 (1994).
  - [25] J. Reinhold *et al.*, Phys. Rev. C **58**, 247 (1998).
  - [26] J. Benlliure, K.-H. Schmidt, D. Cortina-Gil, T. Enqvist, F. Farget, A. Heinz, A.R. Junghans, J. Pereira, and J. Tayeb, Nucl. Phys. **A660**, 87 (1999).
  - [27] V. Foehr *et al.*, Phys. Rev. C **84**, 054605 (2011).
  - [28] M. Mocko *et al.*, Phys. Rev. C **76**, 014609 (2007).
  - [29] M. Pomorski *et al.*, Acta Phys. Pol. **B 43**, 267 (2012).
  - [30] <http://www.gsi.de/documents/FRS-reference-2012-001.html>.